PCCP

PAPER

Cite this: *Phys. Chem. Chem. Phys.*, 2024, **26**, 28617

Photofragmentation and fragment analysis; Coriolis interactions in excited states of CH_3†

Meng-Xu Jiang [ab] and Ágúst Kvaran [*a]

Received 22nd August 2024,
Accepted 30th October 2024

DOI: 10.1039/d4cp03292f

rsc.li/pccp

Methyl radicals in their ground state (CH_3(X)) were created and excited by two- and one- color excitation schemes for CH_3Br and CH_3I, respectively, to record (2+1) REMPI spectra of CH_3 for resonant transitions to the Rydberg states CH_3**(np_z $^2A_2$); n = 3, 4. Various new and previously observed vibrational bands were identified and analyzed to gain energetic information for the Rydberg states. Particular emphasis was placed on analysis of the rotational structured spectra centered at 70 648 and 60 700 cm^{-1}, due to transitions from $v_2'' = 1$ to $v_2' = 1$ and $v_4' = 1$ for both Rydberg states, respectively. Vibrationally forbidden transitions between the v_2'' and v_4' states, gain transition probabilities as a result of mixing of the ν_2 and ν_4 vibrational states due to Coriolis coupling between the two vibrational modes (intensity borrowing effect). As a result, the spectra are dramatically affected, both regarding line intensities and positions. This is the first direct evidence of a Coriolis interaction between two vibrational modes in Rydberg states of CH_3 (and in XH_3 molecules) based on simultaneous observation of spectra due to transitions to both interacting states. The analyses reveal close similarities between the Rydberg states and the ground state cation in terms of energy properties as well as the Coriolis interaction, as evident from comparison with recent work in relation to observation of CH_3^+(X) in space (O. Berné *et al.*, *Nature*, 2023, **621**, 56–59). The effect of Coriolis interactions on predissociation of the Rydberg states/hence fragment products is discussed.

I. Introduction

The methyl radical, CH_3, is one of the most important building block fragment species in organic chemistry and has been found to play an important role in atmospheric,[1] interstellar[2] and combustion[3] chemistry. Its (and its deuterated form CD_3) IR,[4,5] UV,[6–9] Raman[10,11] and REMPI[12–19] spectra have been thoroughly investigated to identify and characterize the ground state[4,5,20] and electronically excited states.[6–9,11–13,15–19] In terms of the electronically excited states the largest emphasis has been on studies of the lowest energy Rydberg states (CH_3**(Ry)), 3s $^2A_1$,[9–11,19,21] 3p_z $^2A_2$[13,15–18,21,22] and 4p_z $^2A_2$[13,14] with respect to spectroscopic properties[9,11,13–19,21] and predissociation.[10,11,14,16–19,21,22] The 3s and np_z (n = 3,4) states are typically accessed by one- (absorption) and two- (REMPI) photon excitations from the ground state CH_3(X $^2A_2$), respectively. Both Rydberg state spectra[11,12,15] and photoelectron spectra[23] show a strong propensity for preservation of the vibrational states. The CH_3(X) (and CD_3(X)) radicals have been created by means of photolysis,[6,7,9–11,14,15,19–21,24–26] discharging,[4,16] pyrolysis[12,13,18] or reactions,[13,17,27] prior to its studies or as a part of its formation analysis. Judging from observed spectra, CH_3(X) is dominantly formed in the zero vibrational state and the ν_2 (out-of-plane bending/OPLA) vibrational mode,[4,11,13,15,17,20,24,26,27] while other vibrational modes are typically formed as ν_1(symmetric stretch) > ν_3(asymmetric stretch), ν_4(deformation).[17,26] Photolysis of CH_3I[10,11,14,15,19,24,25] and CH_3Br,[10,25] by one-photon excitations in the A-bands of the molecules are commonly used in the studies of CH_3(X) and CH_3**(Ry) and relevant photodissociation studies reveal formation of CH_3(X) in different vibrational states $\left(CH_3\left(X;\ v_1''v_2''v_3''v_4''\right)\right)$ along with the halogen atoms in its ground (I(3/2), Br(3/2)) or spin–orbit excited (I*(1/2), Br*(1/2)) states, depending on the excitation wavelengths for CH_3I[24,28–36] and CH_3Br.[26,37–41]

REMPI dynamic studies of CH_3X for X = I[42] and Br,[43–45] which involve two-photon resonant excitations to Rydberg states (CH_3X**) in series that converge to the ground ionic states (CH_3X^+), can also include one-photon non-resonant excitation to the repulsive valence states (CH_3X*) corresponding to the A-band and three-photon excitations to super-excited Rydberg states ($CH_3X^{\#}$) above the ionization limit (Fig. 1a). The excited state intermediates CH_3X* (for X = I, Br) and CH_3Br**, have been found to dissociate to form $CH_3\left(X;\ v_1''v_2''v_3''v_4''\right) + X/X^*$, while $CH_3I^{\#}$ and $CH_3Br^{\#}$ predominantly form CH_3(X) + I** (I** = Rydberg state iodine atoms)[42]

[a] *Science Faculty, University of Iceland, Dunhagi 3, 107 Reykjavík, Iceland. E-mail: agust@hi.is, mej7@hi.is; Web: https://agust.hi.is/; Tel: +354-525-4800*
[b] *Université Paris-Saclay, CNRS, Institut des Sciences Moléculaires d'Orsay, 91405 Orsay, France*

† Electronic supplementary information (ESI) available. See DOI: https://doi.org/10.1039/d4cp03292f

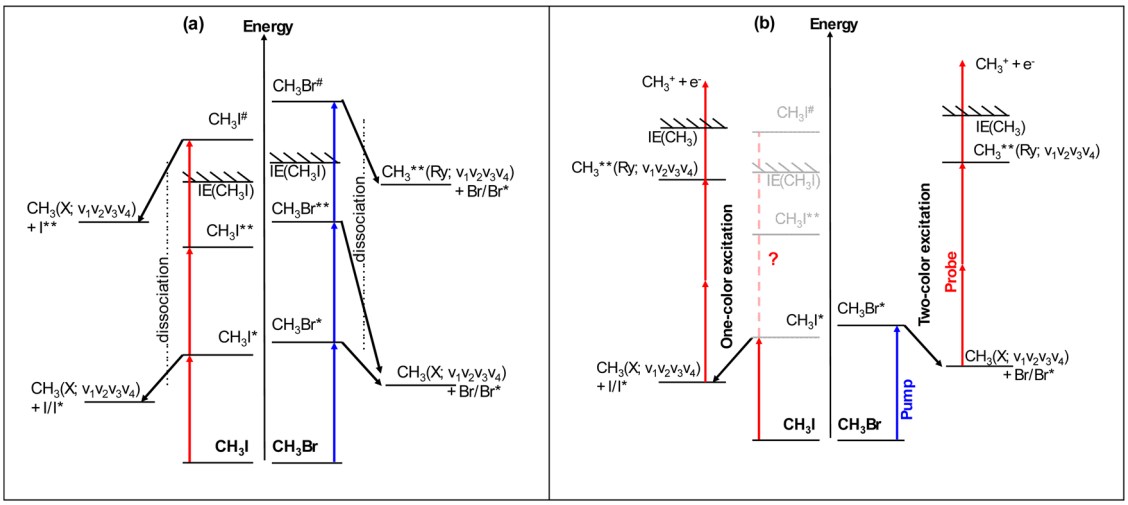

Fig. 1 (a) Schematic figure for multiphoton excitations of CH_3X; X = I, Br and dissociation channels for formation of CH_3(X) and Rydberg states, CH_3**, *via* excitations to repulsive molecular valence states (CH_3X*), Rydberg states (CH_3X**) and superexcited states ($CH_3X^{\#}$) of CH_3X.[42,44] (b) Excitation schemes relevant to the present studies of CH_3(X) (2+1) REMPI *via* Rydberg states, CH_3** for CH_3Br (two-color/pump and probe excitation scheme) and CH_3I (one-color excitation scheme).

and CH_3**(Ry) + Br/Br*,[44] respectively (Fig. 1a). The CH_3 Rydberg states formed in the three-photon excitations of CH_3Br *via* $CH_3Br^{\#}$ depend on the photon energy as well as on the Rydberg electron symmetry (s, p, d) of the intermediate molecular Rydberg state, CH_3Br^{**}.[44]

While the methyl cation, CH_3^+ has long been considered to be an important precursor to organic chemistry in the universe[46–48] it has only recently been discovered in a protoplanetary disk.[49,50] Molecular IR emission detected by the James Webb space telescope from a strongly UV-irradiated medium was identified to be due to rovibrational transitions for the ν_2^+ (OPLA) and ν_4^+ (doubly degenerate in-plane bending) modes within CH_3^+(X) with strong Coriolis interaction between near-degenerate vibrational levels affecting the spectral structure significantly. Since the Rydberg states of CH_3 closely resemble the ground state of CH_3^+ (ref. 23) this discovery prompts consideration of whether Coriolis coupling between the corresponding vibrational modes ν_2 and ν_4 also may exist in CH_3** Rydberg states.

Dynamic and spectroscopic experimental studies of fragment radicals such as CH_3 and its excited states require a selective formation step prior to the analysis of concern. Optimization of the species concentrations and the preferable conditions for the analysis step require simplicity in the initial step and may involve careful adjustment of a time delay between the two steps. In this paper we use a one-color multiphoton excitation scheme for CH_3I and a two-color (pump and probe) excitation scheme for CH_3Br to create $CH_3\left(X;\ v_1''v_2''v_3''v_4''\right)$ by absorption in the A-bands, followed by a CH_3(X) (2+1) REMPI *via* $CH_3^{**}\left(4p_z\ ^2A_2;\ v_1'v_2'v_3'v_4'\right)$ (for CH_3I and CH_3Br) and $CH_3^{**}\left(3p_z\ ^2A_2;\ v_1'v_2'v_3'v_4'\right)$ (for CH_3Br) states (see Fig. 1b). The two-photon resonant excitation $CH_3^{**}(4p_z\ ^2A_2) \leftarrow\leftarrow CH_3(X)$ is in the same wavelength region as the one-photon excitation of $CH_3I^* \leftarrow CH_3I$, while that is not the case for the $CH_3Br^* \leftarrow CH_3Br$ excitation, which explains why the two different excitation schemes are needed. The data allowed comparison of the two different excitation schemes with respect to the quality of the spectral data. Furthermore, the data revealed new spectral observations and state characterizations relevant to the $CH_3^{**}\left(np_z\ ^2A_2(n=3,4);\ v_1'v_2'v_3'v_4'\right) \leftarrow\leftarrow CH_3\left(X;\ v_1''v_2''v_3''v_4''\right)$ transitions, including the first observations of Coriolis couplings between the vibrational modes ν_2 and ν_4 in Rydberg states of CH_3, affecting the spectral structure dramatically and showing clear evidence of intensity borrowing effects. In addition, questions arise, what effects Coriolis interactions can have on fragmentation of CH_3 Rydberg states.

II. Experimental

Two multiphoton excitation schemes were applied to create the methyl radical in its ground state by photolysis of methyl halides, followed by CH_3 (2+1) REMPI *via* resonant excitations to Rydberg states (CH_3**): one-color excitation of CH_3I in the two-photon energy region of 69 500–71 000 cm^{-1} (laser wavelengths 281.70–287.80 nm) and two-color/pump-and-probe excitation of CH_3Br for initial pumping by a fixed wavelength within the A-band of the molecule, followed by probing in the two-photon energy regions of 59 760–60 800 cm^{-1} (laser wavelengths 328.90–334.7 nm) and 69 500–71 000 cm^{-1} (laser wavelengths 281.70–287.80 nm). The experimental apparatus and equipment parameters resembled those described in previous publications.[51–55]

One-color excitation of CH_3I

Photolysis of CH_3I *via* its A-band absorption has emerged as a widely adopted and valuable method for generating the methyl radical (CH_3). This approach is particularly convenient, as the laser wavelengths, 281.70–287.80 nm, necessary for the

two-photon excitation to Rydberg levels in the region of 69 500–71 000 cm^{-1} falls within the A-band continuum. A CH_3I beam was created by a jet expansion of a gas mixture made by flowing argon over a CH_3I liquid sample in a cooled trap, at a backing pressure of about 1 bar through a 500 μm pulsed nozzle into an ionization chamber. The pressure inside the ionization chamber was about 10^{-6} mbar during experiments. The pulsed nozzle was typically kept open for about 140 μs and a laser excitation beam was typically fired 460 μs after its opening. The excitation radiation was generated by a Nd:YAG laser (EKSPLA NL300 Series, 532 nm) pumped Coherent ScanMatePro dye laser followed by a frequency doubling with a BBO crystal. Dyes R610 and R590 were used. The laser beam was focused on the molecular beam by a 200 mm quartz focal lens between a repeller and extractor plates.

Two-color excitation of CH_3Br

Two laser systems consisting of pump lasers, dye lasers and frequency doubling units were used for the two-color excitation experiments. A CH_3Br beam was generated by a jet expansion of a diluted gas mixture containing CH_3Br in argon, typically with a CH_3Br : Ar ratio of about 1 : 1 to 1 : 5 for a backing pressure of 3 bar through a 500 μm pulsed nozzle into an ionization chamber. The pressure inside the ionization chamber was about 10^{-6} mbar during experiments. The pump laser excitation for photolysis of CH_3Br was generated by a Lambda Physik COMPex 205 Excimer laser pumped Lumonics Hyperdye 300 dye laser followed by a frequency doubling with a BBO crystal. Dyes C480 and C503 were used. Fixed wavelengths within the A-band of CH_3Br were chosen, typically 253 nm and 240 nm, prior to $CH_3(X)$ excitations to the $3p_z$ and $4p_z$ states, respectively. The probe laser system was the same as that used in the one-color excitation scheme described above. Dyes R610, R590 and DCM were used. The probe laser pulses were delayed relative to the photolysis pulse on the ns time scale by a time delay unit (Quantum Pulse Generator 9520 series), a necessary disposition to optimize experimental conditions and ensure that an adequate density of photofragments had accumulated before the REMPI detection and/or to minimize ''fly-out'' of the photofragments. Typically, the delay was set to approximately 10 ns. The laser beams were focused on the molecular beam by 200 mm quartz focal lenses between a repeller and extractor plates.

For both excitation schemes ions were directed into a 70 cm long time-of-flight (TOF) tube and detected by a microchannel plate (MCP) detector to record the ion yield as a function of mass and laser radiation wavenumber. Signals were fed into a LeCroy WaveSurfer 44 MXs-A, 400 MHz storage oscilloscope. To prevent saturation effects and power broadening the laser power was minimized. Laser wavenumber calibration was based on observed iodine atomic (2+1) REMPI lines. The accuracy of the calibration was typically found to be about ±2.0 cm^{-1} on the two-photon wavenumber scale.

III. Results and analysis

CH_3 formation and spectra

Fig. 2 shows CH_3 (2+1) REMPI spectra derived from CH_3Br (two-color, pump and probe excitations; Fig. 2a) and CH_3I (one-color excitations; Fig. 2b; see also Fig. S1 in ESI† (ref. 56)) for the two-photon excitation regions of 59 760–60 800 cm^{-1} and 69 500–71 000 cm^{-1}, respectively (see also close up Fig. S2, S4 and S5 of spectra in ESI† (ref. 56)). Comparison with previous observations[13,14,17,27] allows identification of

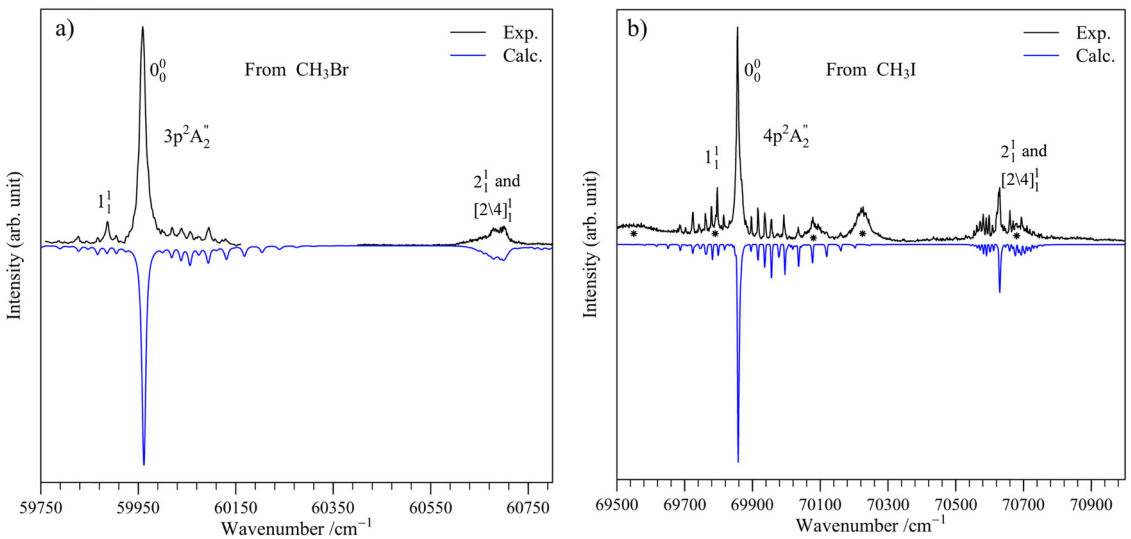

Fig. 2 Experimental (black, top) and calculated (blue, below) $CH_3(X)$ (2+1) REMPI spectra for resonant excitations to the CH_3**(np_z $^2A_2$) Rydberg states, n = 3 (a) and n = 4 (b), following one-photon ionization to form CH_3^+. Experimental spectra are obtained by two-color/pump and probe excitation of CH_3Br (pump wavelength 253 nm) (a) and by one-color excitation of CH_3I (b). Vibrational transitions (0_0^0, 1_1^1, 2_1^1 and $[2\backslash4]_1^1$) are indicated (see main text). Overlapping broad spectral features of CH_3^+ signals following resonant excitations to Rydberg states of CH_3I are marked by * in (b). Rotational lines of calculated spectra are presented as Voigt shaped peaks with linewidths of 8 cm^{-1} (a) and 3 cm^{-1} (b).

spectra due to the transitions $CH_3^{**}(3p_z\ ^2A_2;\ v_1'v_2'v_3'v_4') \leftarrow\leftarrow CH_3(X;\ v_1''v_2''v_3''v_4'')$ for the vibrational transitions (0000) ← ← (0000) (*i.e.* 0_0^0; ν_0 = 59 972 cm^{-1}),[13] (1000) ← ← (1000) (1_1^1; ν_0 = 59 881 cm^{-1})[17] and (0100) ← ← (0100) (2_1^1; ν_0 = 60 700 cm^{-1})[13] and due to $CH_3^{**}(4p_z\ ^2A_2;\ 0000) \leftarrow\leftarrow CH_3(X;\ 0000)$ (0_0^0; ν_0 = 69 853 cm^{-1}).[14] In addition to these spectra, a band peaking at 70 648 cm^{-1}, about 791 cm^{-1} higher than the 0_0^0 band centre peak of the $CH_3^{**}(4p_z\ ^2A_2) \leftarrow\leftarrow CH_3(X)$ transition at 69 857 cm^{-1}, is observed. This we assign to the corresponding 2_1^1 band based on the analogy with the 0_0^0 and 2_1^1 bands of the $CH_3^{**}(3p_z\ ^2A_2) \leftarrow\leftarrow CH_3(X)$ transitions, which are separated by about 728 cm^{-1} (see more detail below).[13] Furthermore, a band, prominently sticking out at 69 796 cm^{-1} about 61 cm^{-1} lower than the 0_0^0 band peak of the $CH_3^{**}(4p_z\ ^2A_2) \leftarrow\leftarrow CH_3(X)$ transition at 69 857 cm^{-1}, is observed. This is assigned to the corresponding 1_1^1 band based on the analogy with the 0_0^0 and 1_1^1 bands of the $CH_3^{**}(3p_z\ ^2A_2) \leftarrow\leftarrow CH_3(X)$ transitions, which are separated by about 77 cm^{-1} (see also Table 1). In addition to the observed CH_3 band spectra, broad spectral features are seen only in the spectra derived from CH_3I (see Fig. 2b). Mass resolved REMPI spectra reveals the same spectral features for the CH_3I^+ and I^+ ions, allowing for identification of some spectra overlapping (underlying) the CH_3 bands (see Fig. 2b). These common broad spectral features indicate two-photon resonant excitations to CH_3I Rydberg states (CH_3I^{**}) followed by further excitation and branching processes to form the ions, CH_3^+, CH_3I^+ and I^+, thus being an indirect measure of two-photon absorptions due to the $CH_3I^{**} \leftarrow\leftarrow CH_3I(X)$ transition. This is in accordance with our earlier observations based on analysis of ion and electron slice images recorded for lower energy REMPI excitations of CH_3I *via* CH_3I^{**},[42] which revealed further one-photon excitation of CH_3I^{**} to superexcited state(s) ($CH_3I^{\#}$),

$$CH_3I^{**} + h\nu \rightarrow CH_3I^{\#} \quad (1)$$

followed by the branching (2) and photoexcitation (3) processes,

$$CH_3I^{\#} \rightarrow CH_3(X) + I^{**};\quad \text{dissociation} \quad (2a)$$

$$CH_3I^{\#} \rightarrow \mathbf{CH_3^+} + I^-;\quad \text{ion-pair dissociation} \quad (2b)$$

$$CH_3I^{\#} \rightarrow \mathbf{CH_3I^+} + e^-;\quad \text{autoionization} \quad (2c)$$

$$I^{**} + h\nu \rightarrow \mathbf{I^+} + e^-;\quad \text{photoionization} \quad (3a)$$

$$CH_3I^+ + h\nu \rightarrow \mathbf{CH_3^+} + I/I^*\quad \text{photodissociation} \quad (3b)$$

where I** are iodine atom Rydberg states. Thus, most likely, the ion formation channels (2b) and (3b) are responsible for the broad CH_3^+ signals, while channels (2c) and (3a) are responsible for the corresponding CH_3I^+ and I^+ signals, respectively (see ions highlighted in bold above). No overlapping (underlying) CH_3^+ spectral features, analogous to those observed in the one-color excitation scheme for CH_3I, were observed in the two-color excitation for CH_3Br. This is probably mainly due to the fact that negligible two-photon resonant excitations to CH_3Br^{**}, followed by further excitation and branching processes to form CH_3^+, are to be expected in the region of the (2+1) REMPI probing of $CH_3(X)$.[44,45,57,58] The different nature of the two-color excitation scheme for CH_3Br (compared to the one-color excitation scheme for CH_3I), where $CH_3(X)$ is initially formed by pumping with a fixed wavelength chosen within the A-band of the parent molecule, followed by scanning at longer wavelengths after a time delay and optimization of conditions to detect $CH_3(X)$ (2+1) REMPI, could also be important. Considering also that the major channels following resonant excitations *via* Rydberg states within CH_3I and CH_3Br involve further $CH_3(X)$ formation along with I** for CH_3I[41] but CH_3^{**} Rydberg states along with Br/Br* for CH_3Br[44] (see Section I), the $CH_3(X)$ spectra obtained by the use of CH_3Br are due to $CH_3(X;\ v_1''v_2''v_3''v_4'')$ formed by photodissocation in the A-band of CH_3Br only, while those derived from CH_3I could also be affected by other $CH_3(X)$ formation channels as well as the CH_3^+ formation processes mentioned above. Further advantage of the two-color excitation scheme for CH_3Br over the one-color excitation scheme for CH_3I appears in the form of higher resolution spectra (sharper spectral peaks) obtainable in the former case, as a result of less power broadening. The $CH_3(X)$ spectra (Fig. 2) were further analyzed and simulated as described in the following section (see also ESI† (ref. 56)).

Table 1 Band origin, ν^0 (cm^{-1}) and assignments of spectra (see main text) due to transitions from the ground state to the $3p_z\ ^2A_2''$ and $4p_z\ ^2A_2''$ Rydberg states of CH_3. The numbers in parentheses are distances (in cm^{-1}) from the 0_0^0 transitions

	$3p_z\ ^2A_2''$				$4p_z\ ^2A_2''$			
Assignment	Others work		This work		Others work		This work	
1_1^1	59 898[a]	(−76)	59 886	(−77)			69 796	(−61)
	59 881[b]	(−73)						
0_0^0	59 974[a]	(0)	59 963	(0)	69 837[b]	(0)	69 857	(0)
	59 954[b]	(0)			69 853[d]	(0)		
	59 972[c]	(0)						
2_1^1	60 688[a]	(714)	60 711	(748)			70 648	(791)
	60 670[b]	(716)						
	60 700[c]	(728)						
$[2\backslash4]_1^1$			60 741	(778)			70 637	(780)

[a] Ref. 27. [b] Ref. 17. [c] Ref. 26. [d] Ref. 14.

Spectral simulations

The CH_3 spectral structure, mentioned above, was simulated by using the PGOPHER program.[59] While the calculated spectra are based on the absorption cross sections for transitions between the states involved $(CH_3^{**}(Ry;\ v_1'v_2'v_3'v_4') \leftarrow\leftarrow CH_3(X;\ v_1''v_2''v_3''v_4''))$ only, the REMPI spectra depend on additional ionization of $CH_3^{**}(Ry;\ v_1'v_2'v_3'v_4')$, which is not known in detail. This could cause some differences in line intensities while peak positions are not affected. Therefore, main emphasis was laid on matching peak positions (more than line intensities) of calculated and experimental spectra in the simulations. Energy levels ($E(N,K)$) of the states involved as a function of the rotational quantum number, N and the quantum number for the projections of the total angular momentum along the molecular symmetry axis (K) could be described, to a first approximation, as follows,[13,16,59–61]

$$E(N,K) = T_v + F(N,K) \quad (4a)$$

$$F(N,K) = BN(N+1) + (C-B)K^2 - D_N N^2(N+1)^2 - D_{NK}N(N+1)K^2 - D_K K^4 - 2C\zeta lK \quad (4b)$$

for all terms in cm^{-1} to give the transition wavenumber (ν), for the energy difference between levels in the Rydberg states ($E(N',K')$) and the ground state ($E(N'',K'')$),

$$\upsilon = \upsilon^0 + (F(N',K') - F(N'',K'')) \quad (4c)$$

where T_v is the vibrational state energy, $F(N,K)$ is the rotational energy and ν^0 is the band origin. The first five terms in eqn (4b) include standard spectroscopic terms for a symmetric top molecule (rotational constants, B, C, D_N, D_{NK} and D_K), the parameters given in ref. 4 and 62 for the ground state, the zero vibrational state and the vibrational mode ν_2, respectively were used (see Table 2). The last term in eqn (4b) represents a Coriolis interaction strength between near-degenerate vibrational levels, used when appropriate (see below). ζ is the Coriolis coupling coefficient and l (= ±1) is related to the vibronic angular momentum, defined based on molecular symmetry.[59] Relevant two-photon selection rules for rotational transitions between two electronic states are,[13]

– for parallel transitions:

$$\text{for } K = 0, \quad \Delta N = 0, \pm2, \quad \Delta K = 0$$

$$\text{for } K \neq 0, \quad \Delta N = 0, \pm1, \pm2, \quad \Delta K = 0 \quad (5a)$$

– for perpendicular transitions:

$$\Delta N = 0, \pm1, \pm2, \quad \Delta K = +1, \quad \Delta l = +1$$

$$\Delta N = 0, \pm1, \pm2, \quad \Delta K = -1, \quad \Delta l = -1 \quad (5b)$$

The matrix elements due to Coriolis interactions between the two vibrational modes ν_2 and ν_4 in excited states for rotational levels of equal quantum numbers (N) for both vibrational states, as a function of N, K and l, for two-photon resonant excitation are expressed as,[59]

$$\langle v_2, N, K \pm 1, l \pm 1 | \hat{H}_{int} | v_4, N, K, l \rangle = \sqrt{N(N+1) - K(K \pm 1)}\{F_{ab} \pm F_{ab,c}(2K \pm 1)\} \quad (6)$$

where $\hat{H}_{int}$ is the interaction operator and F_{ab} and $F_{ab,c}$ are interaction strength parameters. The different signs ($\pm$) refer to shifts of the rotational levels in opposite directions, affecting the positions of corresponding spectral lines. In addition to line shifts, interaction can cause alterations in line intensities in the form of intensity borrowing, as a result of the state mixing.

(a) The 0_0^0 bands of the $CH_3^{**}(np_z\ ^2A_2) \leftarrow\leftarrow CH_3(X)$; n = 3,4, transitions.

The 0_0^0 bands for the $CH_3^{**}(np_z\ ^2A_2) \leftarrow\leftarrow CH_3(X)$; n = 3,4, transitions both show a strong Q line in the middle and much weaker partly separated rotational lines of the O and P series on its short wavenumber side and the R and S series on its long wavenumber side (Fig. 2). Simulations of the rotational structure of the 0_0^0 bands for the parallel $CH_3^{**}(np_z\ ^2A_2) \leftarrow\leftarrow CH_3(X)$; n = 3,4, transitions (Fig. 2) gave spectroscopic parameters for the zero vibrational states of the $CH_3^{**}(3p_z\ ^2A_2)$ and $CH_3^{**}(4p_z\ ^2A_2)$ Rydberg states in good agreement with values derived by Heinze *et al.*[16] and Black *et al.*,[14] respectively (Table 2; see also ESI† (ref. 56)).

Rotational line widths, which are believed to be affected by predissociation of the Rydberg states,[14,16,21] were found to be larger for the 0_0^0 band of the $3p_z$ Rydberg state than of the $4p_z$ state for comparable experimental conditions (see Fig. 2), with minimum FWHM of about 4.3 cm^{-1} for the $3p_z$ state but about 2.4 cm^{-1} for the $4p_z$ state. This suggests that the $3p_z$ state is undergoing faster predissociation than the $4p_z$ state.

(b) The 2_1^1 and $[2\backslash4]_1^1$ bands of the $CH_3^{**}(4p_z\ ^2A_2) \leftarrow\leftarrow CH_3(X)$ transition.

The spectrum in the two-photon excitation region of 70 520–70 750 cm^{-1} resembles the structure of the 0_0^0 bands by showing

Table 2 Spectroscopic parameters for vibrational states of the ground- (top), $3p_z\ ^2A_2''$ and $4p_z\ ^2A_2''$ states of CH_3 and for $CH_3^+(X)$ (bottom) (see main text). All values are in cm^{-1} except for ζ, which is dimensionless. Detaild description of the parameter derivations and uncertainties for the $v_2' = 1$ and $v_4' = 1$ states are given in ESI[56]

Parameters		Ref.	T_v	B	C	$D_N \times 10^4$	$D_{NK} \times 10^4$	$D_K \times 10^4$	ζ	F_{ab}	$F_{ab,c}$
$\tilde{X}\ ^2A_2''$	$v'' = 0$	[a]	0	9.578	4.738	7.95	−14.46	6.873			
	$v_2'' = 1(a_1')$	[b]	606.45	9.258	4.811	4.94	−7.06	2.57			
$3p_z\ ^2A_2''$	$v' = 0$	[c]	59 972	9.51	4.62	7.7	−13.6	6.3			
		This work	59 963	9.47	4.84	9.4	−3.9	6.7			
	$v_2' = 1(a_1')$	This work	61 318	9.18	4.2						
	$v_4' = 1(e'')$	This work	61 348	9.96	4.6				−0.1	−8.9	0.02
$4p_z\ ^2A_2''$	$v' = 0$	[d]	69 853	9.9	4.65	10.7	−21.2	0			
		This work	69 857	9.84	4.8	0.9	16.3	8.9			
	$v_2' = 1(a_1')$	This work	71 254	9.64	4.8	41.2					
	$v_4' = 1(e'')$	This work	71 243	9.78	4.51	−17.4			−0.14	−9.2	0.04
$\tilde{X}^+\ ^1A_1'$	$v^+ = 0$	[e]	79 357.3	9.361	4.615	7.26	−13.07	6.29			
	$v_2^+ = 1(a_2'')$	[e]	80 763.0	9.349	4.634	3.98	7.2	3.75			
	$v_4^+ = 1(e')$	[e]	80 752.5	9.449	4.571	8.09	−13.7	6.16	−0.1	−8.9	0.02

[a] Ref. 61. [b] Ref. 4. [c] Ref. 16. [d] Ref. 14. [e] Ref. 50.

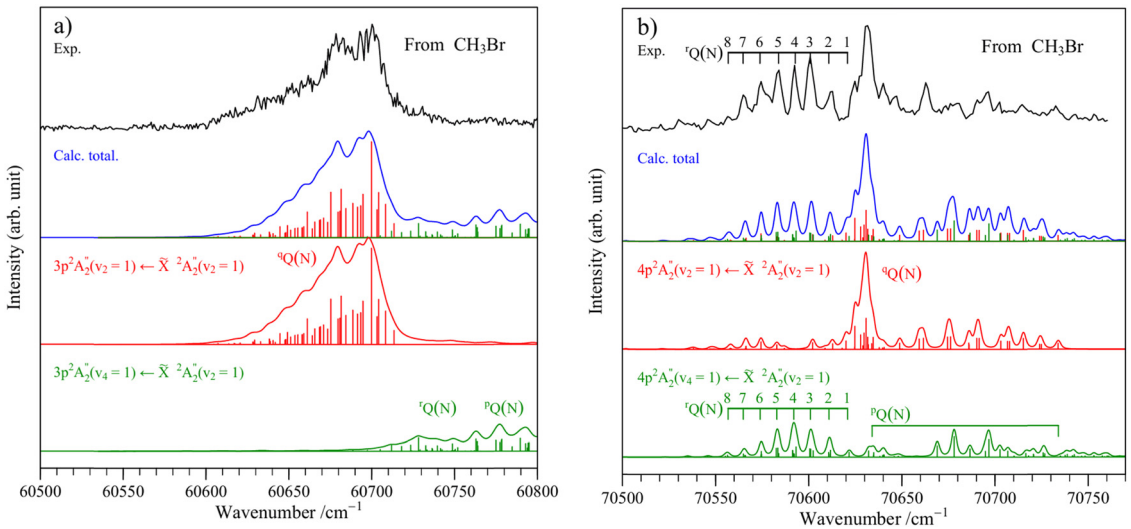

Fig. 3 Experimental (black, top) and calculated (below) $CH_3(X)$ (2+1) REMPI spectra for resonant excitations to the $CH_3^{**}(np_z\ ^2A_2)$ Rydberg states, n = 3 (a) and n = 4 (b), vibrational transitions 2_1^1 and $[2\backslash4]_1^1$, following one-photon ionization to form CH_3^+. Experimental spectra are obtained by two-color/pump and probe excitation of CH_3Br (pump wavelengths, 253 nm (a) and 240 nm (b)). Rotational lines of calculated spectra are presented as sticks and as Voigt shaped peaks with linewidths of 8 cm^{-1} (a) and 3 cm^{-1} (b). Major rotational line series (Q lines) are indicated (see main text).

a broad peak in the centre (70 648 cm^{-1}) with wings of rotational lines on both sides (Fig. 3b). This spectrum, initially assigned to the 2_1^1 band of the $CH_3^{**}(4p_z\ ^2A_2) \leftarrow\leftarrow CH_3(X)$ parallel transition, as mentioned above, could not be simulated based on that assumption alone.[56] An assumption of an additional perpendicular transition to a state close in energy, interacting by Coriolis coupling, on the other hand, allowed the total structure to be simulated. This additional band we assign to the transition $CH_3^{**}(4p_z\ ^2A_2;\ 0001) \leftarrow\leftarrow CH_3(X;\ 0100)$, *i.e.* a transition from the vibrational state $v_2'' = 1$ in the ground state to the vibrational state $v_4' = 1$ in the $4p_z\ ^2A_2$ state, involving Coriolis coupling between the corresponding ν_2 and ν_4 modes in the excited state. This we label as the $[2\backslash4]_1^1$ band, which overlaps the 2_1^1 band. While this transition is forbidden, according to the basic vibrational selection rule of "no alterations in vibrational modes" the state mixing, as a result of the Coriolis coupling, enhances the transition probability of the $[2\backslash4]_1^1$ transition and likewise diminish the transition probability for the 2_1^1 transition, *i.e.*, causes an intensity borrowing effect (see related work of ours in ref. 54 and references therein). The simulation of the combined rotational structure of the 2_1^1 and $[2\backslash4]_1^1$ bands for the $CH_3^{**}(4p_z\ ^2A_2) \leftarrow\leftarrow CH_3(X)$ transition is shown in Fig. 3b and the corresponding spectroscopic constants are listed in Table 2 (see also ESI† (ref. 56)). Fig. 3b shows how the total structure is built up of the two spectral bands 2_1^1 and $[2\backslash4]_1^1$, separated by only about 11 cm^{-1}. The mixing of the two states, which is inversely proportional to the states/bands separation, is large enough to result in comparable total intensities of the 2_1^1 band ($I(2_1^1)$) and the $[2\backslash4]_1^1$ band ($I([2\backslash4]_1^1)$) ($I(2_1^1) : I([2\backslash4]_1^1) \sim 3:2$), corresponds to a large intensity borrowing effect. The Coriolis coupling between the two states acts in the form of level-to-level repulsion for levels of same K and N quantum numbers, inversely proportional to the level's energy difference, to cause line shifts depending on the Coriolis coupling strength (see Fig. 4a, left). Thus, two "interacting levels" are "pushed" in opposite energy directions, as demonstrated in Fig. 4b (right). Furthermore, line intensities vary, depending on the interaction strength parameters (F_{ab} and $F_{ab,c}$). Q lines dominate over much weaker O, P, R and S lines. The 2_1^1 band is mainly composed of Q lines ($\Delta N = 0$) for $\Delta K = 0$ (q lines), marked as $^qQ(N)$, while the $[2\backslash4]_1^1$ band is mainly composed of Q lines ($\Delta N = 0$) for $\Delta K = -1$ (p lines) and $\Delta K = +1$ (r lines), marked as $^pQ(N)$ and $^rQ(N)$ lines, respectively (see Fig. 3b and 4b). A particularly prominent line series on the short wavenumber side of the center peak in the region of about 70 550–70 625 cm^{-1} turns out to be made, to a large extent, of $^rQ(N)$ rotational lines of the $[2\backslash4]_1^1$ band for N = 1–8, K'' = 0–7 (ΔK = +1). Due to limited resolution of the spectrum the spectroscopic parameters of the excited state could not be determined with high precision. In the simulation procedure the Coriolis interaction parameters (ζ, F_{ab} and $F_{ab,c}$) were kept close to those determined for the corresponding ν_2^+ *vs.* ν_4^+ interaction in the ground state ion, $CH_3^+(X)$.[50] This is a justifiable assumption due to the structural similarities between $CH_3^+(X)$ and the Rydberg state $CH_3^{**}(4p_z\ ^2A_2)$, which can be viewed as an ion core with an orbiting 4p Rydberg electron at a far distance, to a first approximation (*i.e.* $[CH_3^+]$ 4p) (see also ref. 23). Furthermore, the interaction parameters depend on the energy difference between the vibrational levels of the two vibrational modes, ν_2 and ν_4, which is found to be similar (about 10 cm^{-1} and 11 cm^{-1} for CH_3^+ and $CH_3^{**}(4p_z\ ^2A_2)$, respectively).

Rotational linewidths are found to be comparable to that for the 0_0^0 band of the $CH_3^{**}(4p_z\ ^2A_2) \leftarrow\leftarrow CH_3(X)$ transition, but smaller than for the 0_0^0 band of the $CH_3^{**}(3p_z\ ^2A_2) \leftarrow\leftarrow CH_3(X)$ transition for comparable experimental conditions, suggesting that the rate of predissociation of the $v_2' = 1$ and $v_4' = 1$ vibrational states are comparable to those of the zero vibrational state in $CH_3^{**}(4p_z\ ^2A_2)$, but less than for the zero vibrational state of $CH_3^{**}(3p_z\ ^2A_2)$.

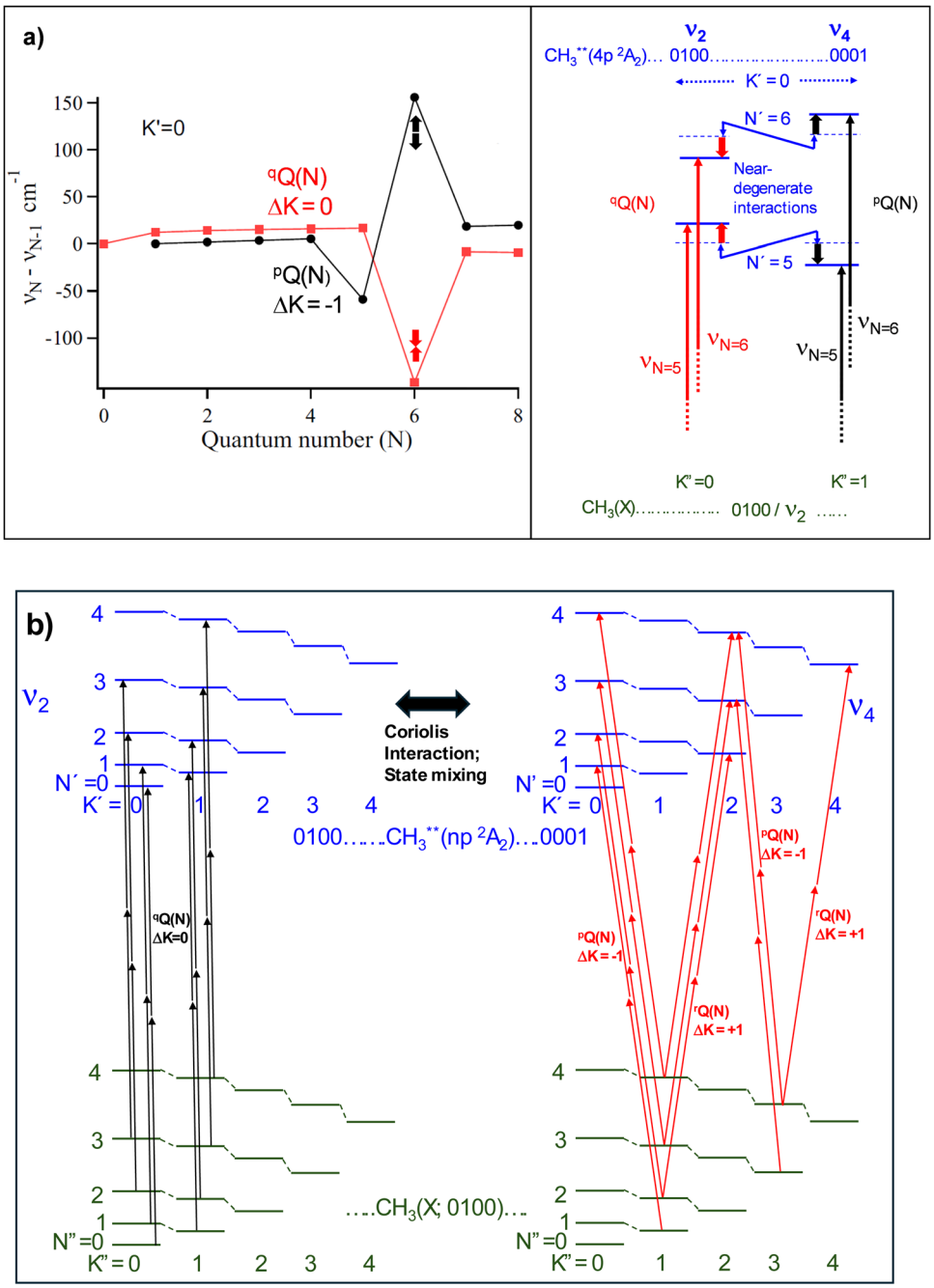

Fig. 4 Energy perturbations (a) and dominant two-photon excitations (b) in transitions to interacting ν_2 and ν_4 vibrational modes in $CH_3^{**}(np_z\ ^2A_2)$; n = 3, 4. (a), Left: Wavenumber differences between rotational lines $^qQ(N)$ and $^pQ(N)$ for K' = 0, ΔN = 1, derived from spectral simulations of the 2_1^1 and $[2\backslash4]_1^1$ bands for the transition $CH_3^{**}(4p_z\ ^2A_2) \leftarrow\leftarrow CH_3(X)$ (see main text and ref. 56). (a) Right: Schematic representation of the energy level shifts for N' = 6 and 5 of the ν_2' and ν_4' vibrational states for K' = 0, as a result of level-to-level repulsion between near-degenerate levels due to a Coriolis interaction between the vibrational modes, according to the line differences to the left. The arrows in the figure on left refer to the corresponding arrows in the figure on right. (b) Schematic representation of rotational energy levels for $CH_3(X)$ and CH_3^{**} (oblate symmetric top) and examples of transitions which dominate in transitions between levels of interacting vibrational states of the vibrational modes ν_2 and ν_4 for parallel ($^qQ(N)$ lines; black arrows to left) and perpendicular ($^pQ(N)$ and $^rQ(N)$ lines; red arrows to right) transitions.

(c) The 2_1^1 and $[2\backslash4]_1^1$ bands of the $CH_3^{**}(3p_z\ ^2A_2) \leftarrow\leftarrow CH_3(X)$ transition.

The spectrum in the two-photon excitation region of about 60 560–60 800 cm^{-1}, peaking at about 60 700 cm^{-1}, which has been assigned to the 2_1^1 band of the $CH_3^{**}(3p_z\ ^2A_2) \leftarrow\leftarrow CH_3(X)$ transition,[13] does not show a resolved rotational structure (Fig. 3a). The spectral shape, however, could not be simulated based on that assumption alone,[56] while assuming a $[2\backslash4]_1^1$ band close by and a Coriolis interaction between the $v_2' = 1$ and $v_4' = 1$ vibrational states, analogous to the corresponding

$CH_3^{**}(4p_z\ ^2A_2)$ system described in the previous paragraph, allowed it to be simulated (Fig. 3a). The limited resolution of the spectrum, however, did neither allow determination of precise spectroscopic constant nor interaction parameters. Instead, the same Coriolis interaction parameters (ζ, F_{ab} and $F_{ab,c}$) as those determined for the corresponding ν_2^+ *vs.* ν_4^+ interaction in $CH_3^+(X)$ were used.[50] Furthermore, the rotational constants D_N, D_{NK} and D_K were set to zero to allow only three variables (T_v, B and C) for the fitting procedure. The simulation is shown in Fig. 3a and the spectroscopic constants are listed in Table 2 (see also ESI† (ref. 56)). The bands are now separated by about 30 cm^{-1}, compared to only about 11 cm^{-1} for the $CH_3^{**}(4p_z\ ^2A_2)$ state (see above). Due to the larger separation the mixing of the two vibrational states is less than for the $CH_3^{**}(4p_z\ ^2A_2)$ state, which appears in the form of larger total intensity ratio of the two bands of about $I(2_1^1) : I([2\backslash4]_1^1) \sim 5:1$, compared to the ratio of 3 : 2 for the $CH_3^{**}(4p_z\ ^2A_2)$ state, corresponding to a less intensity borrowing effect. The 2_1^1 band is mainly made of Q lines for $\Delta K = 0$ (marked as $^qQ(N)$), while the $[2\backslash4]_1^1$ band is mainly made of Q lines for $\Delta K = -1$ and $\Delta K = +1$, marked as $^pQ(N)$ and $^rQ(N)$ lines, respectively as shown in Fig. 3a. Judging from the spectral simulation (see Fig. 3a) the lack of resolved rotational structure in the spectrum is due to high density of rotational lines with considerable linewidths.

While linewidths could not be determined from the simulation with acceptable accuracy, the overall structure could be simulated by assuming comparable linewidths as used for the simulation of the 0_0^0 band of the $CH_3^{**}(3p_z\ ^2A_2)$ system. This might suggest that the rate of predissociation of the $v_2' = 1$ and $v_4' = 1$ vibrational states are comparable to that of the zero vibrational state within $CH_3^{**}(3p_z\ ^2A_2)$.

IV. Discussions

The observation of Coriolis couplings between the two vibrational modes ν_2 and ν_4 within the Rydberg states $CH_3^{**}(np_z\ ^2A_2$; $n = 3,4)$, as evident from a combined spectral simulation of the 2_1^1 and $[2\backslash4]_1^1$ bands, is an outstanding result of the data interpretation presented in the previous section. No such direct evidence of Coriolis interactions, based on simultaneous analysis of spectra due to transitions to both interacting vibrational modes, has been identified before, neither in $CH_3(X)$ nor CH_3^{**}. Coriolis interactions between vibrational modes either within the same electronic states or between different electronic states for XY_3 symmetric top molecules have long been known to exist.[63,64] Numerous evidences for such interactions between bound and repulsive excited states, to cause predissociations, typically appearing in the form of spectral line broadening, have been found for CH_3,[14,16] NH_3[60] and SiH_3.[65] Spectral analyses relevant to either of the two interaction modes have revealed Coriolis interactions in the ground states of CH_3,[4,6,7] NH_3,[63] SiH_3[66] and BH_3[61] or in the excited states of CH_3^{**} (ref. 67) and NH_3^{**}.[60] Thus, large anharmonicity observed for the ν_2 mode in the ground state of CH_3 in IR laser spectra[4] allowed an evaluation of the Coriolis coefficient ($\zeta = 0.67697$).[67] While Hudgens *et al.* observed Coriolis interaction within the $CH_3^{**}(nf\ ^2E)$ (and $CD_3^{**}(nf\ ^2E)$) state they could not find a significant Coriolis interaction within the $CH_3^{**}(3p_z\ ^2A_2)$ (and $CD_3^{**}(3p_z\ ^2A_2)$) state, from rotational structure analysis of a (2+1) REMPI spectrum for the 0_0^0 band for $CD_3(X)$.[13] The spectrum due to the $CH_3^{**}(3p_z\ ^2A_2) \leftarrow\leftarrow CH_3(X)$ transition, centered near 60 700 cm^{-1}, which has been observed in REMPI,[13,27] has remained inexplicable and tentatively assigned to the 2_1^1 transition only.[13,27]

While a limited rotational structure of the spectrum centered near 60 700 cm^{-1} did not allow a detailed spectroscopic analysis, the corresponding spectrum (2_1^1 band) of the $CH_3^{**}(4p_z\ ^2A_2) \leftarrow\leftarrow CH_3(X)$ transition centered at 70 648 cm^{-1} (Fig. 3b), which we observed, contained more structural information, promising for successful analysis. However, as mentioned before (see Section III), it could not be simulated by assuming it to be solely due to the 2_1^1 transition. Recent analysis of infrared spectra of the methyl cation and rotationally resolved photoelectron spectra of CH_3,[50] in connection with validating observations of radiation from CH_3^+ in a protoplanetary disk,[49] turned out to be a key to solving the spectra analysis. Complex perturbations seen in the CH_3^+ IR spectrum could be fully explained by assuming Coriolis interaction between the ν_2^+ and ν_4^+ vibrational modes within the ionic ground state and the relevant interaction parameters (ζ, F_{ab} and $F_{ab,c}$) were derived. Since the Rydberg states $CH_3^{**}(np_z\ ^2A_2)$ can, to a first approximation, be considered to be made of the ground state ion core with orbiting Rydberg electrons at a far distance ($[CH_3^+(X)]\ np$), there is a reason to believe that similar Coriolis interactions are present in the Rydberg states. Furthermore, one might expect closer similarities between Rydberg states and the ground ionic state as the energy of the Rydberg states increases and approaches the ionization limit. Thus, by applying Coriolis interaction parameters close to those obtained for CH_3^+ (see Table 2) and introducing simultaneous transitions to the two vibrational states $v_2' = 1$ and $v_4' = 1$ in $CH_3^{**}(4p_z\ ^2A_2)$, close in energy, from the same original state ($CH_3(X;\ 0100)$), the spectrum in the region of 70 520–70 750 cm^{-1} could be simulated for an energy difference between the two transitions of about 11 cm^{-1} (Fig. 3b and Table 2), which is comparable to the corresponding energy difference for CH_3^+ of 10 cm^{-1}.[50] Analogously the spectrum in the lower energy region of 60 560–60 800 cm^{-1} (for $CH_3^{**}(3p_z\ ^2A_2)$) could be simulated for larger energy difference between the $v_2' = 1$ and $v_4' = 1$ states of about 30 cm^{-1}. It should be emphasized, however, that even if the overall spectrum of the featureless structure of the $CH_3^{**}(3p_z\ ^2A_2)$ spectrum could not be simulated without taking account of the Coriolis interaction, a single set of spectroscopic parameters could not be derived from the simulation.

Vibrational frequencies (in cm^{-1}) of the ν_1, ν_2 and ν_4 vibrational modes for the $CH_3^{**}(np_z\ ^2A_2;\ n = 3,4)$ states, derived from the band origin (Table 1) and known vibrational frequencies of the ground state ($CH_3(X)$) are listed in Table 3, along with values derived by others for $CH_3^{**}(3p_z\ ^2A_2)$ as well as values for $CH_3(X)$ and $CH_3^+(X)$. As to be expected our ν_2 value

Table 3 Vibrational frequencies (in cm^{-1}) of the ν_1, ν_2 and ν_4 vibrational modes for the CH_3**(np_z $^2A_2$; n = 3,4) states, derived from the analyses of the band origin (Table 1) for known vibrational frequencies of the ground state (CH_3(X)) along with values derived by others for CH_3**($3p_z$ $^2A_2$), CH_3(X) and CH_3^+(X)

State	Ref.	T_v	ν_1	ν_2	ν_3	ν_4
$\tilde{X}$ $^2A_2''$	[a]	0	3004	607	3161	1398
$3p_z$ $^2A_2''$	This work	59 963	2927	1355		1385
	[b]	59 955	2931	1323	3085[c]	(1428)
$4p_z$ $^2A_2''$	This work	69 857	2943	1398		1387
			ν_1^+	ν_2^+	ν_3^+	ν_4^+
$\tilde{X}^+$ $^1A_1'$	[d]	79 355	2943	1405	3109	1395

[a] Ref. 68. [b] Ref. 17. [c] Ref. 69. [d] Ref. 50.

derived for the CH_3**($3p_z$ $^2A_2$) state of ν_2 = 1355 cm^{-1} by taking account of the Coriolis interaction between the two modes differs significantly from the previous determination of ν_2 = 1323 cm^{-1} obtained without considering any interaction.[17] Even greater discrepancy is observed between our value of ν_4 = 1385 cm^{-1} and that determined by Zhang *et al.* of ν_4 = 1428 cm^{-1}, which was estimated from data for CD_3 based on isotope shifts.[17] Our values of ν_2 = 1398 cm^{-1} and ν_4 = 1387 cm^{-1} for the higher energy CH_3**($4p_z$ $^2A_2$) Rydberg states are larger than the corresponding values for the CH_3**($3p_z$ $^2A_2$) state and closer to those for CH_3^+(X) of ν_2^+ = 1405 cm^{-1} and ν_4^+ = 1395 cm^{-1},[17] as one might expect. Our value of ν_1 = 2943 cm^{-1} is identical to the corresponding value derived for ν_1^+ of CH_3^+(X).[50]

Our minimum rotational linewidths (FWHM) of about 4.3 cm^{-1} measured for the 0_0^0 band of the CH_3**($3p_z$ $^2A_2$) ← ← CH_3(X) transition (see above) is in good agreement with previous observations.[16,28] This has been interpreted as being due to a combination of homogeneous and heterogeneous predissociation, of which the heterogeneous component is due to a Coriolis interaction with lower dissociation states to cause bound-to-free transition.[16,21] Our results, that the FWHM for the 0_0^0 and $2_1^1 + [2\backslash4]_1^1$ bands of the CH_3**($4p_z$ $^2A_2$) ← ← CH_3(X) transition are significantly less (about 2.4 cm^{-1}; see above) than for CH_3**($3p_z$ $^2A_2$) ← ← CH_3(X) is also in agreement with other observations.[14] This suggests that analogous predissociation channels for the $4p_z$ state are of less important than for the $3p_z$ state. The large linewidths, hence low resolution, of the $2_1^1 + [2\backslash4]_1^1$ bands affect severely the quality of the parameters derived from the spectral simulations. Judging from linewidths of the 0_0^0 spectra for the $4p_z$ state[14] and lifetime measurements for the $3p_z$ states[22] for CH_3 and CD_3 the linewidths of CD_3 spectra are likely to be smaller than for CH_3. Therefore, although the density of the rotational states is higher for CD_3, recording and analysing the corresponding CD_3**($4p_z$) spectrum might be an alternative choice to improve the quality of the spectroscopic and interaction parameters.

V. Summary, conclusions and closing remarks

CH_3(X) radicals were created and resonant excited in multi-photon excitation of CH_3Br and CH_3I. A two-color pump and probe excitation scheme was used in the case of CH_3Br, by pumping within the A-band of CH_3Br, followed by scanning the two-photon excitation regions of 59 760–60 800 cm^{-1} and 69 500–71 000 cm^{-1}, which cover (2+1) REMPI of CH_3(X) for resonant excitations to the CH_3**($3p_z$ $^2A_2$) and CH_3**($4p_z$ $^2A_2$) vibrational Rydberg states, respectively. A one-color excitation scheme was used for CH_3I, scanning the two-photon excitation region of 69 500–71 000 cm^{-1}, to photoexcite CH_3I as well as to cover (2+1) REMPI of CH_3(X) for resonant excitation to the CH_3**($4p_z$ $^2A_2$) Rydberg state. While the one-color excitation scheme serves both the photolytic generation of CH_3(X) and its probing (Fig. 1), it has the disadvantage that other CH_3^+ REMPI signals, as a result of CH_3^+ formation channels following resonant excitations within CH_3I, overlapping those due to the (2+1) REMPI of CH_3(X) (Fig. 2b). The pump and probe method for CH_3Br allowed better quality CH_3(X) REMPI spectra, as a result of less power broadening, to be recorded.

New as well as previously observed REMPI spectra of CH_3(X),[13,14,17] were identified (Fig. 2) and analyzed (Tables 1 and 2).[13,14,16,17,27] Detailed inspection of spectra centered at 69 796 cm^{-1} and 70 648 cm^{-1} revealed each of these to consist of closely separated bands as a result of transitions to interacting states. These were assigned to transitions from the same initial vibrational state, $v_2'' = 1$ of ground state CH_3(X) to the $v_2' = 1$ (parallel transition, 2_1^1) and $v_4' = 1$ (perpendicular transition, $[2\backslash4]_1^1$) vibrational states of the CH_3**($3p_z$ $^2A_2$) and CH_3**($4p_z$ $^2A_2$) states, respectively, affected by Coriolis couplings between the ν_2 and ν_4 vibrational modes. While the transitions from ν_2 to ν_4 ($[2\backslash4]_1^1$) are vibrationally forbidden the transition probability is enhanced due to the mixing of the two vibrational modes due to the Coriolis coupling. The intensity borrowing effect is inversely proportional to the energy difference between the interacting states (see ref. 54 and references therein), appearing as larger total intensity ratio of the two band contributions ($I(2_1^1) : I([2\backslash4]_1^1)$) for the CH_3**($4p_z$ $^2A_2$) state than for the CH_3**($3p_z$ $^2A_2$) state. The combined spectral structure, due to the two transitions, is dominantly made of Q rotational lines (ΔN = 0) for ΔK = 0 (ν_2 to ν_2/parallel transitions) and $\Delta K = \pm 1$ (ν_2 to ν_4/perpendicular transitions). Spectral perturbations appear as irregularities in the line series due to the interaction in the form of level-to-level repulsions between levels of same rotational quantum numbers within the two vibrational states. Simulations of the combined 2_1^1 and $[2\backslash4]_1^1$ bands allowed evaluation/estimation of spectroscopic parameters for both vibrational states, Coriolis interaction parameters and vibrational frequencies for both vibrational modes.

Judging from the analysis, the Rydberg states of concern closely resemble the ground state methyl cation in terms of the structure and vibrational and rotational properties, as well as the Coriolis interaction between the two vibrational modes, ν_2 and ν_4, as evidenced by comparison with a recent pioneering spectral analysis of CH_3^+(X)[50] in relation to its recent observation in a protoplanetary disk.[49] This is to be expected, since the Rydberg states CH_3**(np_z $^2A_2$) can, to a first approximation, be considered to be made of the ground state ion cores with orbiting Rydberg electrons at far distances ([CH_3^+(X)] np).

Rotational linewidths, determined from the REMPI spectra, indicate a relatively short lifetime (τ) of the Rydberg states, $CH_3^{**}(np_z\ ^2A_2)$ for $\tau(n = 3) < \tau(n = 4)$, due to predissociation of different rates. The predissociation is believed to be due to a combination of parallel and perpendicular transitions to repulsive states involving Coriolis interactions.[16,21] It is, therefore a reason to believe that Coriolis interactions between excited states of CH_3, bound as well as repulsive, can influence the outcome of predissociation and photodissociation channels of CH_3, in terms of fragmentation.

This paper demonstrates how the quality of data sampling relevant to fragment studies can depend on the method of its production by photolysis. Thus, two-color/pump and probe excitation is favored over one-color excitation in the case of spectral analysis of the fragment species of concern here ($CH_3(X)$). Energy properties of the fragment cation in its ground state proved to be an important guideline for predicting the corresponding energy properties of Rydberg states in a series converging to the ion. It allowed identification of spectral bands due to vibrationally forbidden transitions from the ground state to Rydberg vibrational states, with enhanced transition probabilities, hence intensity borrowing effect as a result of mixing with accessible vibrational states due to Coriolis coupling. Thus, the state interactions affect dramatically the spectra appearance. This is the first direct evidence of a Coriolis interaction between two vibrational modes in Rydberg states of CH_3 and in XH_3 type of molecules, based on simultaneous observation of spectra due to transitions to both interacting states. Furthermore, the interactions have implications for dissociation processes of Rydberg states in terms of fragment products. In general, we feel that this paper is important for shedding light on the effect of state interactions within molecules on energetic and fragmentation properties and believe that it can serve as a guideline for further work along those lines in fields such as astrochemistry and combustion.

Author contributions

Meng-Xu Jiang: data curation, formal analysis, funding acquisition, investigation, methodology, writing – review & editing. Ágúst Kvaran: conceptualization, funding acquisition, investigation, methodology, project administration, supervision, validation, writing – original draft, writing – review & editing.

Data availability

Data supporting this article has been included as part of the ESI.† The code for PGOPHER (a program for rotational, vibrational and electronic spectra; C. M. Western, 2018, University of Bristol Research Data Repository) can be found at **https://pgopher.chm.bris.ac.uk/**, doi: **https://doi.org/10.5523/bris.3mqfb4glgkr8a2rev7f73t300c**. The version of the code employed for this study is no. 10.1. Data, relevant to spectral simulations, including experimental and calculated spectra (bands 2_1^1 and $[2\backslash4]_1^1$; see main text) suitable for loading into PGOPHER are available from University of Iceland at, **https://agust.hi.is/CH3/CH3_4p_series.ovr**; **https://agust.hi.is/CH3/CH3_4p_series.pgo**, **https://agust.hi.is/CH3/CH3_3p_series.ovr**; **https://agust.hi.is/CH3/CH3_3p_series.pgo**.

Conflicts of interest

There are no conflicts to declare.

Acknowledgements

The financial support of the University Research Fund, University of Iceland and the Icelandic Research Fund (Grant No. 184693-053) is gratefully acknowledged. Aðalsteinn Kristjánsson's memorial fund for the promotion of natural sciences and chemistry is also acknowledged. We thank Dr Helgi Rafn Hróðmarsson, Dr Ugo Jacovella, Dr Marie-Aline Martin-Drumel, Dr Bérenger Gans and Prof. Séverine Boyé-Péronne for useful discussions.

References

1 K. Riedel and K. Lassey, *Water Atmos*, 2008, **16**, 7170–7176.
2 H. Feuchtgruber, F. Helmich, E. F. van Dishoeck and C. Wright, *Astrophys. J.*, 2000, **535**, L111.
3 K. C. Smyth and P. H. Taylor, *Chem. Phys. Lett.*, 1985, **122**, 518–522.
4 C. Yamada, E. Hirota and K. Kawaguchi, *J. Chem. Phys.*, 1981, **75**, 5256–5264.
5 V. Spirko and P. Bunker, *J. Mol. Spectrosc.*, 1982, **95**, 381–390.
6 G. Herzberg and J. Shoosmith, *Can. J. Phys.*, 1956, **34**, 523–525.
7 G. Herzberg, *Proc. R. Soc. London, Ser. A*, 1961, **262**, 291–317.
8 J. Barnard and A. Duncan, *J. Chem. Phys.*, 1971, **54**, 1760–1762.
9 A. B. Callear and M. P. Metcalfe, *Chem. Phys.*, 1976, **14**, 275–284.
10 S. G. Westre, P. Kelly, Y. Zhang and L. Ziegler, *J. Chem. Phys.*, 1991, **94**, 270–276.
11 S. Westre, T. Gansberg, P. Kelly and L. Ziegler, *J. Phys. Chem.*, 1992, **96**, 3610–3615.
12 T. DiGiuseppe, J. W. Hudgens and M.-C. Lin, *J. Phys. Chem.*, 1982, **86**, 36–41.
13 J. W. Hudgens, T. DiGiuseppe and M.-C. Lin, *J. Chem. Phys.*, 1983, **79**, 571–582.
14 J. F. Black and I. Powis, *J. Chem. Phys.*, 1988, **89**, 3986–3992.
15 D. H. Parker, Z. Wang, M. H. Janssen and D. W. Chandler, *J. Chem. Phys.*, 1989, **90**, 60–67.
16 J. Heinze, N. Heberle and K. Kohse-Höinghaus, *Chem. Phys. Lett.*, 1994, **223**, 305–312.
17 B. Zhang, J. Zhang and K. Liu, *J. Chem. Phys.*, 2005, **122**, 1043101–1043104.
18 H. Fu, Y. Hu and E. Bernstein, *J. Chem. Phys.*, 2005, **123**, 2343071–2343075.

19 T. B. Settersten, R. L. Farrow and J. A. Gray, *Chem. Phys. Lett.*, 2003, **370**, 204–210.
20 D. E. Milligan and M. E. Jacox, *J. Chem. Phys.*, 1967, **47**, 5146–5156.
21 S. M. Poullain, D. V. Chicharro, A. Zanchet, M. G. González, L. Rubio-Lago, M. L. Senent, A. García-Vela and L. Bañares, *Phys. Chem. Chem. Phys.*, 2016, **18**, 17054–17061.
22 G. Balerdi, J. Woodhouse, A. Zanchet, R. de Nalda, M. L. Senent, A. García-Vela and L. Bañares, *Phys. Chem. Chem. Phys.*, 2016, **18**, 110–118.
23 J. Bacon and S. Pratt, *Chem. Phys. Lett.*, 1999, **311**, 346–354.
24 R. Ogorzalek Loo, H.-P. Haerri, G. Hall and P. Houston, *J. Chem. Phys.*, 1989, **90**, 4222–4236.
25 A. Schulenburg, C. Alcaraz, G. Grassi and F. Merkt, *J. Chem. Phys.*, 2006, **125**, 1043101–10431010.
26 F. Wang, M. L. Lipciuc, A. Kartakoullis, P. Glodic, P. C. Samartzis, X. Yang and T. N. Kitsopoulos, *Phys. Chem. Chem. Phys.*, 2014, **16**, 599–606.
27 J. Schlütter, R. Schott and K. Kleinermanns, *Chem. Phys. Lett.*, 1993, **213**, 262–268.
28 D. W. Chandler, J. W. Thoman Jr, M. H. Janssen and D. H. Parker, *Chem. Phys. Lett.*, 1989, **156**, 151–158.
29 L. Rubio-Lago, A. García-Vela, A. Arregui, G. Amaral and L. Bañares, *J. Chem. Phys.*, 2009, **131**, 174309-01–174309-17.
30 Y.-J. Jung, Y. Shin Kim, W. Kyung Kang and K.-H. Jung, *J. Chem. Phys.*, 1997, **107**, 7187–7193.
31 M. González, J. Rodríguez, L. Rubio-Lago, A. García-Vela and L. Bañares, *Phys. Chem. Chem. Phys.*, 2011, **13**, 16404–16415.
32 L. Rubio-Lago, J. Rodríguez, A. García-Vela, M. González, G. Amaral and L. Bañares, *Phys. Chem. Chem. Phys.*, 2011, **13**, 8186–8194.
33 S. M. Poullain, D. V. Chicharro, L. Rubio-Lago, A. García-Vela and L. Bañares, *Philos. Trans. R. Soc., A*, 2017, **375**, 20160205.
34 S. J. Riley and K. R. Wilson, *Faraday Discuss. Chem. Soc.*, 1972, **53**, 132–146.
35 R. O. Loo, G. Hall, H. Haerri and P. Houston, *J. Phys. Chem.*, 1988, **92**, 5–8.
36 E. M. Warne, B. Downes-Ward, J. Woodhouse, M. A. Parkes, D. Bellshaw, E. Springate, P. Majchrzak, Y. Zhang, G. Karras and A. S. Wyatt, *et al.*, *Phys. Chem. Chem. Phys.*, 2019, **21**, 11142–11149.
37 T. Gougousi, P. C. Samartzis and T. N. Kitsopoulos, *J. Chem. Phys.*, 1998, **108**, 5742–5746.
38 J. G. Underwood and I. Powis, *Phys. Chem. Chem. Phys.*, 2000, **2**, 747–756.
39 C. Escure, T. Leininger and B. Lepetit, *J. Chem. Phys.*, 2009, **130**, 2443061–2443068.
40 V. Blanchet, P. C. Samartzis and A. M. Wodtke, *J. Chem. Phys.*, 2009, **130**, 03430401–03430411.
41 W. P. Hess, D. W. Chandler and J. W. Thoman Jr, *Chem. Phys.*, 1992, **163**, 277–286.
42 K. Matthíasson, G. Koumarianou, M.-X. Jiang, P. Glodic, P. C. Samartzis and Á. Kvaran, *Phys. Chem. Chem. Phys.*, 2020, **22**, 4984–4992.
43 F. Wang, M. L. Lipciuc, X. Yang and T. N. Kitsopoulos, *Phys. Chem. Chem. Phys.*, 2009, **11**, 2234–2240.
44 A. Hafliðason, P. Glodic, G. Koumarianou, P. C. Samartzis and Á. Kvaran, *Phys. Chem. Chem. Phys.*, 2018, **20**, 17423–17433.
45 A. Hafliðason, P. Glodic, G. Koumarianou, P. C. Samartzis and Á. Kvaran, *Phys. Chem. Chem. Phys.*, 2019, **21**, 10391–10401.
46 J. Black and A. Dalgarno, *Astrophys. J., Suppl. Ser.*, 1977, **34**, 405–423.
47 D. Smith, *Chem. Rev.*, 1992, **92**, 1473–1485.
48 E. Herbst, *Front. Astron. Space Sci.*, 2021, **8**, 776942.
49 O. Berné, M.-A. Martin-Drumel, I. Schroetter, J. R. Goicoechea, U. Jacovella, B. Gans, E. Dartois, L. H. Coudert, E. Bergin and F. Alarcon, *et al.*, *Nature*, 2023, **621**, 56–59.
50 P. B. Changala, N. L. Chen, H. L. Le, B. Gans, K. Steenbakkers, T. Salomon, L. Bonah, I. Schroetter, A. Canin and M.-A. Martin-Drumel, *et al.*, *Astron. Astrophys.*, 2023, **680**, A19.
51 H. R. Hróðmarsson, H. Wang and Á. Kvaran, *J. Mol. Spectrosc.*, 2013, **290**, 5–12.
52 H. R. Hróðmarsson, H. Wang and Á. Kvaran, *J. Chem. Phys.*, 2014, **140**, 24430401–24430410.
53 H. R. Hróðmarsson and Á. Kvaran, *Phys. Chem. Chem. Phys.*, 2015, **17**, 32517–32527.
54 H. R. Hróðmarsson, H. Wang and Á. Kvaran, *J. Chem. Phys.*, 2015, **142**, 24431201–24431211.
55 M.-X. Jiang and Á. Kvaran, *Phys. Chem. Chem. Phys.*, 2022, **24**, 6676–6689.
56 See ESI†.
57 T. Ridley, J. T. Hennessy, R. J. Donovan, K. P. Lawley, S. Wang, P. Brint and E. Lane, *J. Phys. Chem. A*, 2008, **112**, 7170–7176.
58 A. Kvaran, H. Wang, K. Matthiasson and A. Bodi, *J. Phys. Chem. A*, 2010, **114**, 9991–9998.
59 C. M. Western, *J. Quant. Spectrosc. Radiat. Transfer*, 2017, **186**, 221–242.
60 M. N. Ashfold, R. N. Dixon, N. Little, R. Stickland and C. M. Western, *J. Chem. Phys.*, 1988, **89**, 1754–1761.
61 K. Kawaguchi, *Can. J. Phys.*, 1994, **72**, 925–929.
62 K. Kawaguchi, *Can. J. Phys.*, 2001, **79**, 449–459.
63 V. Spirko, *J. Mol. Spectrosc.*, 1983, **101**, 30–47.
64 I. Mills, *Pure Appl. Chem.*, 1965, **11**, 325–344.
65 R. D. Johnson III, B. P. Tsai and J. W. Hudgens, *J. Chem. Phys.*, 1989, **91**, 3340–3359.
66 V. Špirko, W. Kraemer and J. Burda, *J. Mol. Spectrosc.*, 1991, **147**, 478–487.
67 T. Amano, P. Bernath, C. Yamada, Y. Endo and E. Hirota, *J. Chem. Phys.*, 1982, **77**, 5284–5287.
68 H. F. King and K. Morokuma, *J. Chem. Phys.*, 1979, **71**, 3213–3220.
69 W. Zhang, H. Kawamata, A. J. Merer and K. Liu, *J. Phys. Chem. A*, 2009, **113**, 13133–13138.